East European Journal of Physics. **4.** 177-186 (2024)
DOI:10.26565/2312-4334-2024-4-16 ISSN 2312-4334

MAGNETO HYDRODYNAMIC AND BIO-CONVECTION EFFECTS ON HYBRID NANOFLUID DYNAMICS OVER AN INVERTED ROTATING CONE WITH DIFFERENT BASE FLUIDS

Balaji Padhy[a]*, Archana Senapati[b], Goutam Kumar Mahato[a], P.K. Rath[a]
[a]*Centurion University of Technology and Management, Odisha, India*
[b]*Department of Mathematics, School of Applied Sciences, KIIT Deemed to be University, Bhubaneswar, Odisha, India*
[*]*Corresponding Author e-mail: Balaji.padhy11@gmail.com*
Received July 3, 2024; revised September 17, 2024; in final form September 23, 2024; accepted September 25, 2024

This study explores the combined effects of magnetohydrodynamics (MHD) and bio-convection on the flow dynamics of hybrid Nanofluids over an inverted rotating cone with different base fluids. The hybrid Nanofluids, composed of nanoparticles suspended in various base fluids, exhibit unique thermal and flow characteristics due to the interplay between magnetic fields and bio-convection phenomena. The governing equations, incorporating the principles of MHD and bio-convection, are derived and solved using numerical methods. The analysis considers the impact of key parameters such as magnetic field strength, the rotation rate of the cone, nanoparticle volume fraction, and types of base fluids on the flow behaviour, heat transfer, and system stability. Results indicate that the MHD significantly influences the velocity and temperature profiles of the hybrid Nanofluids, while bio-convection contributes to enhanced mixing and heat transfer rates. Additionally, the choice of base fluid plays a critical role in determining the overall performance of the hybrid Nano fluid system. This study provides valuable insights into optimizing the design and operation of systems utilizing hybrid Nanofluids in applications where MHD and bio-convection effects are prominent.
Keywords: *Magnetohydrodynamics (MHD); Bio-convection; Hybrid nanofluids; Inverted rotating cone; Base fluids; Nanoparticles; Flow dynamics*
PACS: 47.65.-d, 47.63.-b,47.35. Pq,83.50.-v

1. INTRODUCTION

The movement of heat studied in different fields through cones has acquired remarkable research attention owing to its realistic applications in modern life. Appropriate design and application information are crucial for achieving industrial and technological goals. This study explores the combined effects of magnetohydrodynamics (MHD) and bio-convection on the flow dynamics of hybrid nanofluids over an inverted rotating cone with different base fluids. The hybrid nanofluids, composed of nanoparticles suspended in various base fluids, exhibit unique thermal and flow characteristics due to the interplay between magnetic fields and bio-convection phenomena. The governing equations, incorporating the principles of MHD and bio-convection, are derived and solved using numerical methods. The analysis considers the impact of critical parameters such as magnetic field strength, the rotation rate of the cone, nanoparticle volume fraction, and types of base fluids on the flow behaviour, heat transfer, and system stability. Results indicate that the MHD significantly influences the velocity and temperature profiles of the hybrid nanofluids, while bio-convection contributes to enhanced mixing and heat transfer rates. Additionally, the choice of base fluid plays a critical role in determining the overall performance of the hybrid nanofluid system. This study provides valuable insights into optimizing the design and operation of systems utilizing hybrid nanofluids in applications where MHD and bio-convection effects are prominent.

Many researchers have studied the natural convective heat transfer phenomena over vertical cones, focusing on the effects of cone geometry. These investigations have provided valuable insights into optimizing heat transfer in various engineering and industrial applications [1-4]. Liu *et al.[5]*compared cerebral hemodynamic metrics from CFD models using Newtonian and non-Newtonian fluid assumptions to simulate blood flow in intracranial atherosclerotic stenosis (ICAS). Aloliga *et al*.[6] investigates the magnetohydrodynamic boundary layer flow of non-Newtonian Casson fluids over a magnetised, exponentially stretching sheet. Loganathan *et al.* [7] examine the thermally radiative flow of a Casson fluid over a cylinder with velocity slip, suction/injection, and Newtonian heating. Fatunmbi *et al.*[8]Investigates quadratic thermal convection in Magneto-Casson fluid flow influenced by stretchy material, tiny particles, and viscous dissipation effects. Shankar *et al.*[9] investigate Casson fluid flow over an inclined, stretching cylindrical surface, incorporating heat generation, viscous dissipation, thermal radiation, magnetic fields, and mixed convection. Raja *et al.* [10] investigate free convection heat transfer in hybrid nanofluids over an inclined porous plate, considering asymmetrical flow behaviour and sinusoidal heat transfer boundary conditions with an angled magnetic field. Elattar *et al.*[11] studied three-dimensional heat transfer induced by a non-Newtonian Eyring–Powell fluid containing sodium alginate-based CoFe2O4 nanoparticles over a deformable horizontal surface.

Bio-convection, a captivating phenomenon in nanofluids, arises from the motion of microorganisms propelled by swimming. These microorganisms generate a thicker boundary layer that breaks into bio-convection cells, inducing instability and higher density gradients at the surface. Gyrotactic and oxytactic microorganisms represent two distinct types influencing this behaviour. Applications of bio-convection span diverse fields, including pharmaceutical

Cite as: B. Padhy, A. Senapati, G.K. Mahato P.K. Rath, East Eur. J. Phys. 4, 177 (2024), https://doi.org/10.26565/2312-4334-2024-4-16

manufacturing, gas-bearing processes, hydrodynamics research, and wine-making, highlighting its relevance across industrial and scientific domains. Mkhatshwa *et al.* [12] investigates the bio-convective flow of magneto-Williamson nanofluids with motile microbes through a porous medium in a horizontal circular cylinder. Alhussain et al. [13] examine the bioconvective flow of magneto-Williamson nanofluids with motile microbes through a porous medium in a horizontal circular cylinder. Zohra *et al.*[14] analyses about convective anisotropic slip boundary layer flow from a rotating vertical cone in ethylene glycol nanofluid, considering Stefan blowing. The study of Hiemenz and Homann flow over a plate was explored by Sarfraz *et al.* [15].

Upon review, it is evident that the impact of bioconvection on magnetohydrodynamic hybrid nanofluid flow through a rotating cone with distinct base fluids remains unexplored. This study aims to investigate the influence of bioconvection on MHD hybrid nanofluid flow modelled with the Casson fluid approach over a spinning cone.

Key novel aspects of this study include:

- Introduction of motile microorganisms into the flow over a rotating cone.
- Application of MHD effects to a hybrid nanofluid comprising H2O and NaC6H9O7 base fluids.
- In the hybrid nanofluid flow, which consists of Aluminum oxide – Titanium oxide, Titanium oxide – Copper, and Aluminum oxide – Copper hybrid nanoparticles, along with Newtonian (H2O) and non-Newtonian (NaC6H9O7) base fluids, the interactions between these nanoparticles and fluids influence the thermal and flow characteristics significantly. These combinations are crucial for studying enhanced heat transfer and fluid dynamics in various industrial and technological applications.

2. PROPOSED MATHEMATICAL MODEL

Let us consider the incompressible, steady-state boundary layer flow combined with bio-convection phenomena around a rotating downward-pointing vertical cone. The system employs two novel base fluids: Ethanol (C_2H_5OH) and Propylene Glycol ($C_3H_8O_2$), integrated with hybrid nanoparticles composed of Zinc Oxide (ZnO) – Silicon Dioxide (SiO_2), Copper (Cu) – Silver (Ag), and Zinc Oxide (ZnO) – Silver (Ag) combinations. The analysis incorporates surface temperature and concentration gradients and evaluates the system under a generalized magnetic field. Both thermal and concentration boundary conditions are considered, with Newtonian base fluids serving as a reference point. The spatial setup includes the modified Cartesian coordinates where the ξ-axis is along the cone surface, and the η-axis is perpendicular to it. The azimuthal angle α describes the plane rotation around the vertical symmetry axis. A magnetic field of strength $B = B_o\, f(\xi)/\sqrt{1-\xi'^2}$ is applied along the η-axis, and the radius of the cone is given by $r = \xi\, cos\delta$ where δ is the cone's half-angle. We assume thermal equilibrium between the base fluids and nanoparticles, and no slip conditions apply. The study begins with an overview of the bio-convection and hybrid nanofluid systems within the boundary layer. The two novel base fluids, Ethanol and Propylene Glycol, are mixed with nanoparticles for improved heat transfer characteristics. This exploration is conducted under boundary-layer approximations, ensuring that the base fluids and nanoparticles remain in thermal equilibrium with no relative slip by Hassan et al.[16].

The boundary layer equations are derived based on the following assumptions and flow conditions:

$$\frac{\partial}{\partial \xi}(r\,u) + \frac{\partial}{\partial \eta}(rv) = 0. \tag{1}$$

where u and v are velocity components along ξ and η axis, respectively, and $r = \xi\, cos\delta$ represents the cone radius.
Now the momentum equation (for the axial component) is given by

$$\rho hnf\left(u\frac{\partial u}{\partial \xi} + v\frac{\partial u}{\partial \eta} - \frac{w^2}{\xi}\right) = \left(1+\frac{1}{\gamma}\right)\mu hnf\frac{\partial^2 u}{\partial \eta^2} + (\rho\beta_T)hnf\, g\, cos\delta(T-T_0) + (\rho\beta_C)hnf\, g\, cos\delta(C-C_0) - \sigma_{hnf}B^2u. \tag{2}$$

The Azimuthal momentum equation is given by

$$\rho hnf\left(u\frac{\partial w}{\partial \xi} + v\frac{\partial w}{\partial \eta} - \frac{uw}{\xi}\right) = \left(1+\frac{1}{\gamma}\right)\mu_{hnf}\frac{\partial^2 w}{\partial \eta^2} - \sigma_{hnf}B^2w. \tag{3}$$

The Energy equation (temperature distribution) is given by

$$(\rho C_p)hnf\left(u\frac{\partial T}{\partial \xi} + v\frac{\partial T}{\partial \eta}\right) = k_{hnf}\frac{\partial^2 T}{\partial \eta^2}. \tag{4}$$

The Species concentration equation is given by

$$u\frac{\partial C}{\partial \xi} + v\frac{\partial C}{\partial \eta} = D_B\frac{\partial^2 C}{\partial \eta^2}. \tag{5}$$

The Microorganism concentration equation is given by

$$u\frac{\partial n}{\partial \xi} + v\frac{\partial n}{\partial \eta} - \frac{\partial}{\partial \eta}\left(n\frac{\partial C}{\partial \eta}\right)\frac{PW_c}{C_r - C_0}\frac{L}{\xi} = D_n\frac{\partial^2 n}{\partial \eta^2}. \tag{6}$$

The boundary condition for current flow system are as follows:
At the cone surface $\eta = 0$;

$$u = 0, v = 0, w = r\Omega, T = T_0 + (T_r - T_0)\frac{\xi}{L}, C = C_0 + (C_r - C_0)\frac{\xi}{L}, n = n_0 + (n_r + n_0)\frac{\xi}{L}. \quad (7)$$

At $\eta \to \infty$:

$$\mathrm{u} \to 0, w \to 0, T \to T_0, C \to C_0 \; and \; n \to n_0. \quad (8)$$

The hybrid nanofluid properties are redefined in terms of the volume fractions φ_{np1} (for the first nanoparticle) and φ_{np2} (for the second nanoparticle):

$$\mu_{hnf} = \frac{\mu_f}{(1-\phi_{np1})^{2.5}(1-\phi_{np2})^{2.5}}. \quad (9)$$

$$\rho_{hnf} = \{(1 - \phi_{np2})[(1 - \phi_{np1})\rho_f + \phi_{np1}\rho_{np1}]\} + \phi_2\rho_{np2} \quad (10)$$

$$\alpha_{hnf} = \frac{k_{hnf}}{(\rho C_p)_{hnf}}. \quad (11)$$

The heat capacity of a hybrid nanofluid is calculated by using a weighted average of the specific heat capacities of the base fluid and the nanoparticles.

$$(C_p)_{hnf} = \frac{(1-\phi_{np1}-\phi_{np2})(\rho C_p)_f + \phi_{np1}(\rho C_p)_{np1} + \phi_{np2}(\rho C_p)_{np2}}{(1-\phi_{np1}-\phi_{np2})\rho_f + \phi_{np1}\rho_{np1} + \phi_{np2}\rho_{np2}}. \quad (12)$$

The thermal expansion coefficient of the hybrid nanofluid can be approximated as a volume-weighted sum of the thermal expansion coefficients of the base fluid and the nanoparticles:

$$(\beta_T)_{hnf} = (1 - \phi_{np1} - \phi_{np2})(\beta_T)_f + \phi_{np1}(\beta_T)_{np1} + \phi_{np2}(\beta_T)_{np2}. \quad (13)$$

The thermal conductivity of a hybrid nanofluid is more complex to model due to the interaction between nanoparticles and the base fluid. A common model is based on Maxwell's effective medium theory, which can be extended to hybrid nanofluids as follows:

$$k_{hnf} = k_f \left[\frac{k_{np1}+2k_f-2\phi_{np1}(k_f-k_{np1})}{k_{np1}+2k_f+\phi_{np1}(k_f-k_{np1})}\right]\left[\frac{k_{np2}+2k_f-2\phi_{np2}(k_f-k_{np2})}{k_{np2}+2k_f+\phi_{np2}(k_f-k_{np2})}\right]. \quad (14)$$

The electrical conductivity of hybrid nanofluids is enhanced due to the addition of nanoparticles, and can also be modelled using Maxwell's effective medium theory, similar to the thermal conductivity. The electrical conductivity σ_{hnf} is given by:

$$\sigma_{hnf} = \sigma_f \left[\frac{\sigma_{np1}+2\sigma_f-2\phi_{np1}(\sigma_f-\sigma_{np1})}{\sigma_{np1}+2\sigma_f+\phi_{np1}(\sigma_f-\sigma_{np1})}\right]\left[\frac{\sigma_{np2}+2\sigma_f-2\phi_{np2}(\sigma_f-\sigma_{np2})}{\sigma_{np2}+2\sigma_f+\phi_{np2}(\sigma_f-\sigma_{np2})}\right]. \quad (15)$$

To further simplify the equations, the following dimensionless variables are introduced: (Alhussain et al.0, Aghamajidi et al. [17])

$$\xi = \frac{\xi^*}{L}, \eta = \frac{\eta^*}{L}, u = \frac{u^*}{L}, v = \frac{v^*}{L}, w = \frac{w^*}{\Omega L}, \Theta = \frac{T-T_0}{T_r-T_0}, \varphi = \frac{C-C_0}{C_r-C_0}, \chi = \frac{n-n_0}{n_r-n_0}. \quad (16)$$

Solve the equation from 1-6 and applying equation (16), we get

$$u\frac{\partial w}{\partial \xi} + v\frac{\partial w}{\partial \eta} + uw\frac{r'}{r} = \frac{1}{\left[(1-\phi_{np2})\left[1-\phi_{np1}+\phi_{np1}\frac{\rho_{np1}}{\rho_f}\right]+\phi_{np2}\frac{\rho_{np2}}{\rho_f}\right]}\left\{\frac{1}{(1-\phi_{np1})^{2.5}(1-\phi_{np2})^{2.5}}\left(1+\frac{1}{\beta}\right)\frac{\partial^2 w}{\partial \eta^2} - \frac{\sigma_{hnf}}{\sigma_f}M\Lambda^2 w\right\}. \quad (17)$$

$$u\frac{\partial \Theta}{\partial \xi} + v\frac{\partial \Theta}{\partial \eta} = \frac{1}{Br}\left\{\frac{1}{(1-\phi_{np2})\left[1-\phi_{np1}+\phi_{np1}\frac{(\rho C_p)_{np1}}{(\rho C_p)_f}\right]+\phi_{np2}\left(\frac{(\rho C_p)_{np2}}{(\rho C_p)_f}\right)}\right\}\frac{k_{hnf}}{k_f}\frac{\partial^2 \Theta}{\partial \eta^2}. \quad (18)$$

$$u\frac{\partial \varphi}{\partial x} + v\frac{\partial \varphi}{\partial y} = \frac{1}{Sc}\frac{\partial^2 \varphi}{\partial y^2}. \quad (19)$$

$$u\frac{\partial \chi}{\partial x} + v\frac{\partial \chi}{\partial y} = \frac{1}{Lb}\frac{\partial^2 \chi}{\partial y^2} - \frac{1}{x}\frac{Pe}{Lb}\left[\frac{\partial \chi}{\partial y}.\frac{\partial \varphi}{\partial y} + \chi\frac{\partial^2 \varphi}{\partial y^2}\right]. \quad (20)$$

After applying initial conditions, we get the following differential equations

$$\frac{1}{(1-\phi_{np1})^{2.5}(1-\phi_{np2})^{2.5}}\left(1+\frac{1}{\beta}\right)W'' + [2VW' - 2V'W]\left[(1-\phi_{np2})\left[1-\phi_{np1}+\phi_{np1}\frac{\rho_{np1}}{\rho_f}\right]+\phi_{np2}\frac{\rho_{np2}}{\rho_f}\right] - \frac{\sigma_{hnf}}{\sigma_f}M\Lambda^2 W = 0. \quad (21)$$

$$X'' + Pr\left[\left(1-\phi_{np2}\right)\left[1-\phi_{np1}+\phi_{np1}\frac{(\rho C_p)_{np1}}{(\rho C_p)_f}\right]+\phi_{np2}\left(\frac{(\rho C_p)_{np2}}{(\rho C_p)_f}\right)\right]\left[\frac{k_f}{k_{hnf}}\right][2VX' - V'X] = 0. \tag{22}$$

$$Y'' + Sc\,[2VY' - V'Y] = 0. \tag{23}$$

$$Z'' - Pe\,[Z'Y' + ZY''] + Lb[2VZ' - V'Z] = 0. \tag{24}$$

Again, apply the following boundary conditions we obtained

$$V = 0,\ V' = 0,\ W = 1,\ X = 1,\ Y = 1,\ Z = 1 \quad at \quad y = 0,$$

$$V' \to 0,\ W \to 0,\ X \to 0, \qquad Y \to 0, \qquad Z \to 0 \quad as \quad y \to \infty. \tag{25}$$

3. Numerical Method: 4th-Order Runge-Kutta and Shooting Technique

The 4th-order Runge-Kutta method is used to solve this system of first-order ODEs. The steps of this method are as follows:

Step 1: Start with initial guesses for the unknown boundary values at $y = 0$(for example, y_2, y_4, y_6, ...etc., for the velocity, temperature, etc.).

Step 2: Integrate the system of ODEs using the Runge-Kutta method from $y = 0$ to a large value of y (denoted as $y = \infty$) where the boundary conditions at infinity are applied.

Step 3: Compare the computed values at $y = \infty$ with the boundary conditions at infinity (e.g. $y_2(\infty),\ y_4(\infty),\ y_6(\infty)$, ..., etc.).

Step 4: Adjust the initial guesses iteratively using the shooting technique until the boundary conditions at infinity are satisfied to a desired level of accuracy.

4. Transformation of Governing Equations to First-Order ODEs

To apply numerical methods such as the 4th-order Runge-Kutta method, the system of second- and third-order ODEs needs to be transformed into a system of first-order ODEs.

The ODEs derived from the governing equations are expressed in terms of the functions V(y), W(y), X(y), Y(y), and Z(y), which describe the radial velocity, axial velocity, temperature, concentration, and microorganism distribution, respectively. These functions are transformed into first-order ODEs using the following designations:

$$V = y_1, V' = y_2, V'' = y_3, W = y_4, W' = y_5, X = y_6, X' = y_7, Y = y_8,\ Y' = y_9, Z = y_{10},\ Z' = y_{11}.$$

Using these designations, the system of equations (21)-(25) is transformed into the following set of first-order ODEs:

1. For the radical velocity V:

$$y_1' = y_2\ , y_2' = y_3$$

$$y_3' = \left(1+\frac{1}{\beta}\right)^{-1}\left(\left(1-\phi_{np1}\right)^{2.5}\left(1-\phi_{np2}\right)^{2.5}\right)$$

$$\left\{\begin{array}{l} -[2y_1y_3 - {y_2}^2 + \varepsilon {y_4}^2]\left[\left(1-\phi_{np2}\right)\left[1-\phi_{np1}+\phi_{np1}\frac{\rho_{np1}}{\rho_f}\right]+\phi_{np2}\frac{\rho_{np2}}{\rho_f}\right]+\frac{\sigma_{hnf}}{\sigma_f}M\Lambda^2 y_2 \\ \quad -\left[\left(1-\phi_{np2}\right)\left[1-\phi_{np1}+\phi_{np1}\frac{(\rho\beta_T)_{np1}}{(\rho\beta_T)_f}\right]+\phi_{np2}\frac{(\rho\beta_T)_{np2}}{(\rho\beta_T)_f}\right][y_6 + Ncy_8 + Nny_{10}] \end{array}\right\} \tag{26}$$

2. For the axial velocity W:

$$y_4' = y_5$$

$$y_5' = \left(1+\tfrac{1}{\beta}\right)^{-1}\left(\left(1-\phi_{np1}\right)^{2.5}\left(1-\phi_{np2}\right)^{2.5}\right)\left[\frac{\sigma_{hnf}}{\sigma_f}M\Lambda^2 y_4 - \left[\left(1-\phi_{np2}\right)\left[1-\phi_{np1}+\phi_{np1}\frac{\rho_{np1}}{\rho_f}\right]+\phi_{np2}\frac{\rho_{np2}}{\rho_f}\right][2y_1y_5 - 2y_2y_4]\right]. \tag{27}$$

3. For the temperature X:

$$y_6' = y_7$$

$$y_7' = -\Pr\left[\frac{k_f}{k_{hnf}}\right][2y_1y_7 - y_2y_6]\left[\left(1-\phi_{np2}\right)\left[1-\phi_{np1}+\phi_{np1}\frac{(\rho C_p)_{np1}}{(\rho C_p)_f}\right]+\phi_{np2}\left(\frac{(\rho C_p)_{np2}}{(\rho C_p)_f}\right)\right]. \tag{28}$$

4. For the concentration Y:

$$y_8' = y_9,\ y_9' = -Sc[2y_1y_9 - y_2y_8]. \tag{29}$$

5. For the microorganism distribution Z:

$$y_{10}' = y_{11}$$

$$y_{11}' = Pe[y_{11}y_9 + y_{10}(-Sc[2y_1y_9 - y_2y_8])] - Lb[2y_1y_{11} - y_2y_{10}]. \tag{30}$$

The boundary conditions are translated into the following form for the system of first-order ODEs:
At $y = 0$,

$y_1(0) = 0,\ y_2(0) = 0, y_4(0) = 1,\ y_6(0) = 1,\ \ y_8(0) = 1,\ \ y_{10}(0) = 1,$

At $y = \ \infty$,

$y_2(\infty) = 0,\ \ y_4(\infty) = 0,\ \ y_6(\infty) = 0,\quad y_8(\infty) = 0,\ \ y_{10}(\infty) = 0.$

5. NUMERICAL EXAMPLE

In this section, we will analyse the sensitivity of the system to various flow parameters by examining their effects on Sherwood number, Nusselt number, and skin friction. The parameters considered include:

1. Magnetic Parameter (M)
2. Volume Fraction of Nanoparticles (ϵ)
3. Bioconvection Parameters (Nc,Nn)
4. Schmidt Number (Sc)

Example: Consider the following parameter values based on the typical setup for nanofluid flow:

$$M = 1, Nc = 0.1 = Nn, Sc = 0.6, Pr = 6.5, \varphi_{np1} = 0.005, \varphi_{np2} = 0.015, \epsilon = 1\ , \Lambda = 1, \beta = 1$$

These values represent a non-Newtonian fluid with bio-convection and magnetohydrodynamic.
Sol: The 4th-order Runge-Kutta method is used to integrate the system from $y = 0$ to a sufficiently large value of $y_\infty = 10$. To apply iteration procedure, we get numerical solution for $y_1(y), y_2(y), y_3(y), \ldots., y_{10}(y), y_{11}(y)$. These correspond to the velocity, temperature, concentration, and microorganism profiles.

Table 1. The effect of varying flow parameters on the Sherwood number for both Newtonian and non-Newtonian base fluids. This analysis focuses on how changes in parameters such as M, ϵ, Nc, Nn, and Sc influence the Sherwood number in the presence of different nanoparticle combinations.

M	Nc	Nn	Sc	$Al_2O_3 - TiO_2$	$TiO_2 - Cu$	$Al_2O_3 - Cu$	ϵ	$F''(0)$ Ajhamajidi	$F''(0)$ Modified
1	0.1	0.1	0.1	0.20434	0.20490	0.20489	0.0	0.65	0.65
	0.5			0.19424	0.19457	0.19456			
	0.9			0.18905	0.18928	0.18928			
1	0.1	0.1	0.1	0.20434	0.20490	0.20489	0.2	0.73	0.70
		0.3		0.21337	0.21382	0.21382			
		0.6		0.22576	0.22604	0.22604			
1			0.1	0.20434	0.20490	0.20489	0.4	0.82	0.77
			0.4	0.30051	0.30244	0.30242			
			0.7	0.37883	0.38183	0.38179			
1	0.1	0.1	0.1	0.20395	0.20451	0.20451	0.6	0.89	0.85
1	0.1	0.1	0.1	0.20375	0.20430	0.20429	0.8	0.96	0.93
1	0.1	0.1	0.1	0.20734	0.20774	0.20774	1.0	1.02	1.00

6. SENSITIVITY ANALYSIS

This section has explored the impact of different factors on bio-convection and steady two-dimensional magnetohydrodynamic (MHD) free convection in Casson nanofluid flow over a spinning cone.
Figure 1. (a-c), Figure 2. (a-c), and Table 1.

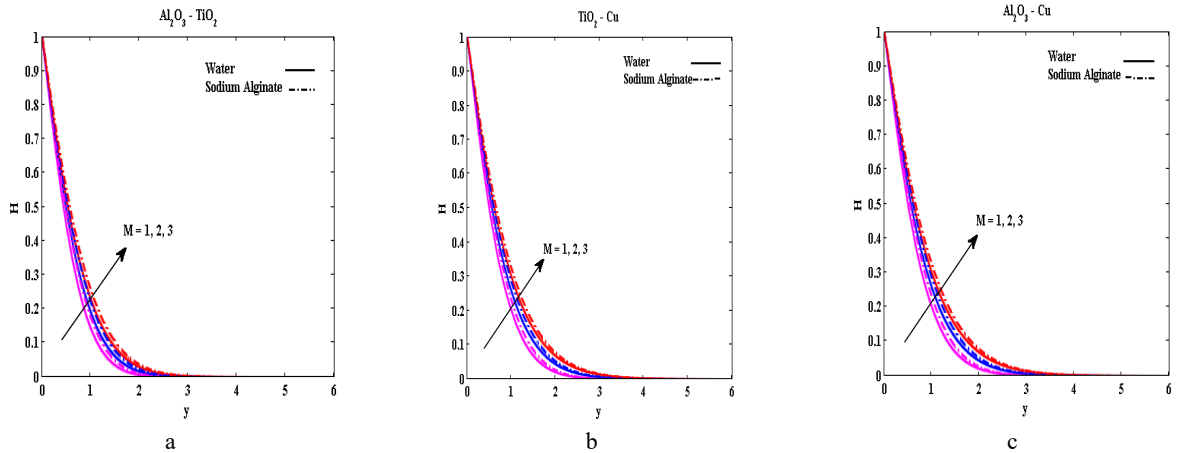

Figure 1. (a-c) Graph of M on the temperature profile

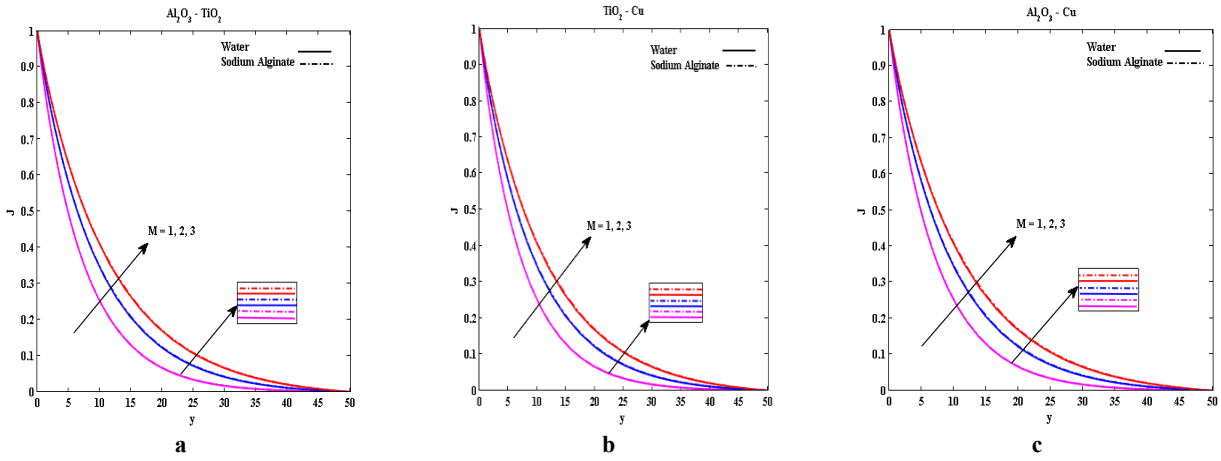

Figure 2. (a-c) Graph of M on the microorganism profile

- Figs. 1(a-c) and 2(a-c) were analyzed to observe heat and motile microorganism profiles across a wide range of magnetic parameters (M = 1, 2, 3) in hybrid nanofluids.
- As the magnetic parameter (M) increases, both temperature and motile microorganism profiles show an increase in hybrid nanofluids.
- it is demonstrated that the thermal and motile microorganism boundary layer thicknesses increase due to the release of additional heat in the hybrid nanofluids as the magnetic parameter (M) is increased.
- Furthermore, it is demonstrated that non-Newtonian-based hybrid nanofluids outperform Newtonian-based ones. This superiority is attributed to sodium alginate, which exhibits a significantly higher Prandtl number and thermal diffusivity compared to water-based hybrid nanofluids.

Figure 3. (a-c), Figure 4. (a-c) and Table 1.

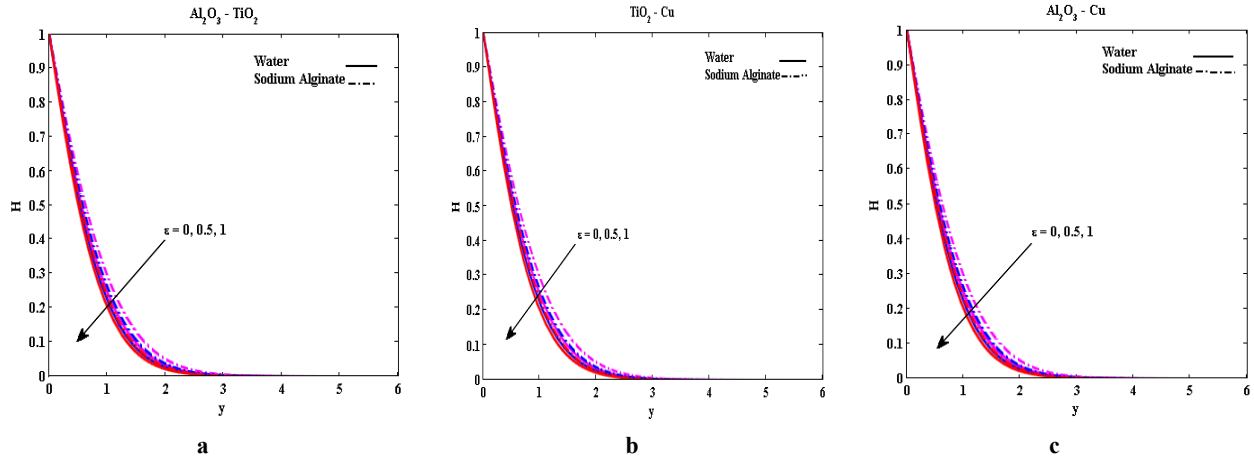

Figure 3. (a-c) Graph of ε on the temperature profile

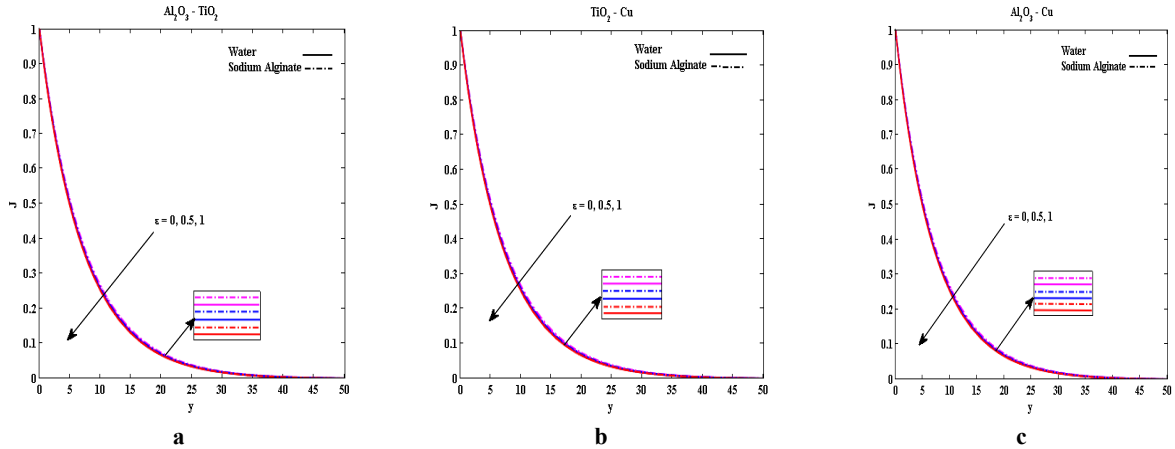

Figure 4. (a-c) Graph of **ε** on the microorganism profile

- It illustrates the impact of spin parameter (ε = 0, 0.5, 1) on temperature and microorganism species density profiles in hybrid nanofluids.
- The heat profiles (Fig. 3 (a-c)) and microorganism profiles (Fig. 4 (a-c)) show a decreasing trend across all three hybrid nanofluids as the spin parameter ε increases.
- This decline is attributed to the thinning of the boundary layer as ε increases. The Newtonian base fluid exhibits a similar decline in thermal expansion within the hybrid nanofluids.
- Graph depict variations in microorganism species density for different values of Nc (Nc = 0.1, 0.5, 0.9) (from Fig. 5.).
- The microorganism profiles show symmetrical motion of hybrid nanoparticles with various base fluids and a tendency to aggregate. Non-Newtonian base fluids exhibit faster acceleration compared to Newtonian base fluids, resulting in a reduction in flow patterns within hybrid nanofluids.
- **Figure 5. (a-c) and Table 1.**

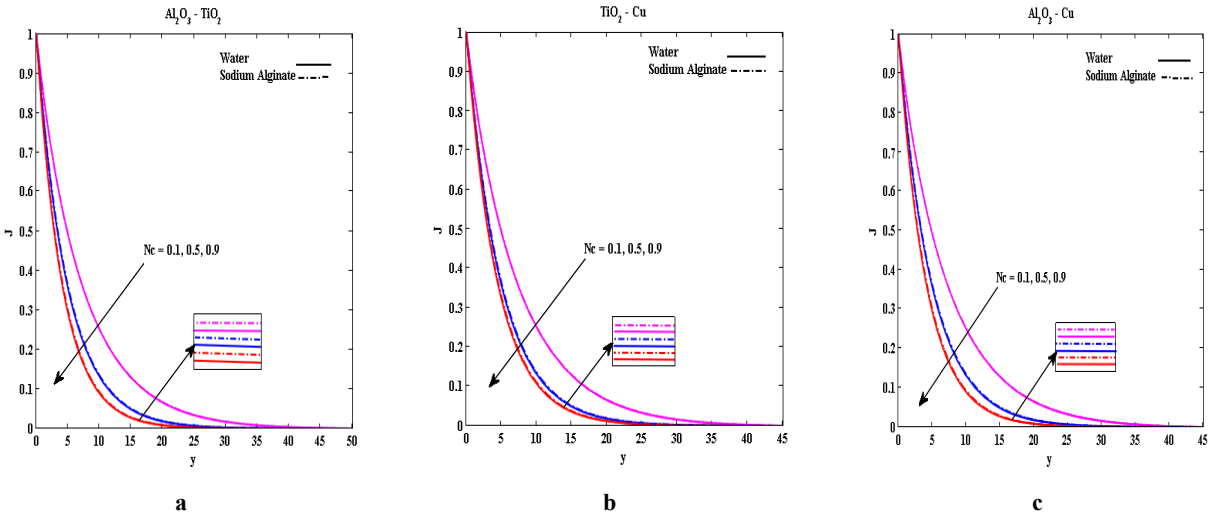

Figure 5. (a-c) Graph of Nc on the microorganism profile

Figure 6. (a-c) and Table 1.

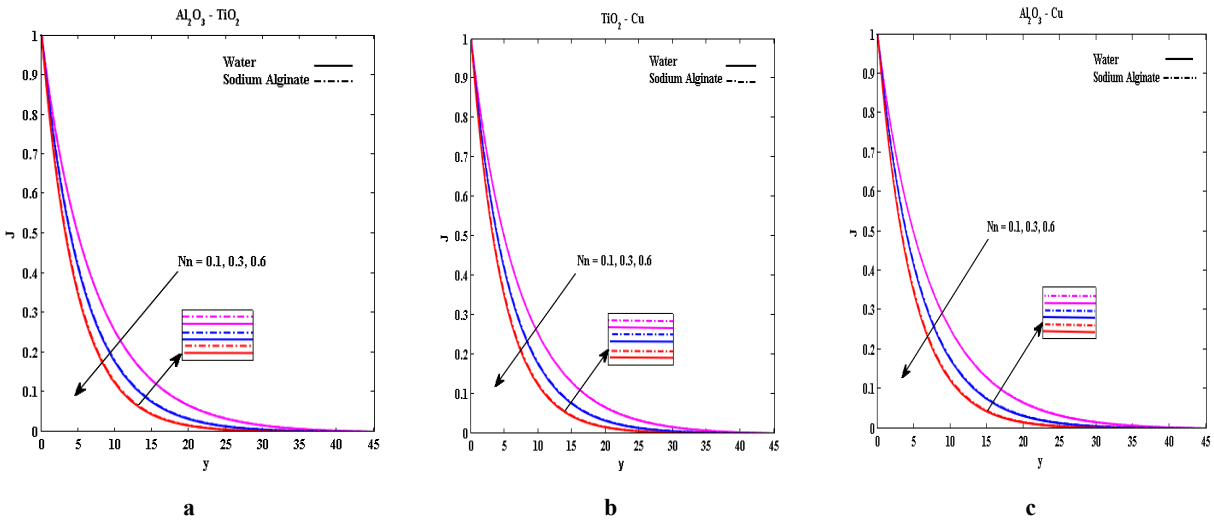

Figure 6. (a-c) Graph of Nn on the microorganism profile

- Graph (Fig-6) illustrate the impact of hybrid nanoparticles with Nn values (Nn = 0.1, 0.3, 0.6) on the microorganism species density profile using two base fluids.
- The buoyancy effects associated with increasing Nn result in a significant decrease in microorganism species density across all three hybrid nanofluids. Non-Newtonian base fluids exhibit more excellent acceleration, leading to stiffening of the boundary layer as Nn increases in the three hybrid nanoparticles.

Figure 7. (a-c) and Table 1.

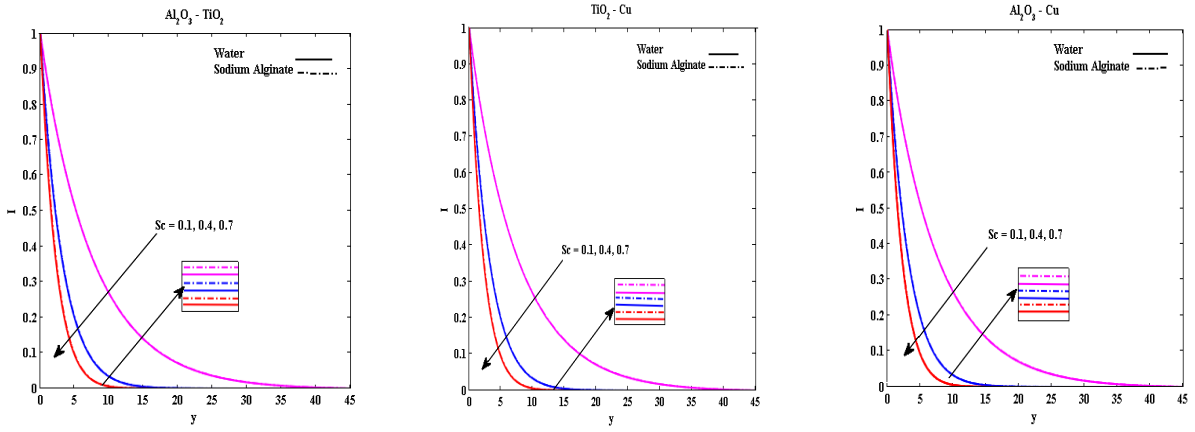

Figure 7. (a-c) Graph of Sc on the concentration profile

- Graph illustrates the influence of Schmidt number Sc (Sc = 0.1, 0.4, 0.7) on the concentration flow fields in hybrid nanofluids. The concentration profiles (Fig. 7(a-c)) show a decrease as Sc increases, reflecting a reduction in mass diffusion due to the ratio of momentum diffusivity to mass diffusivity.

Figure 8 (a-c) and Table 1.

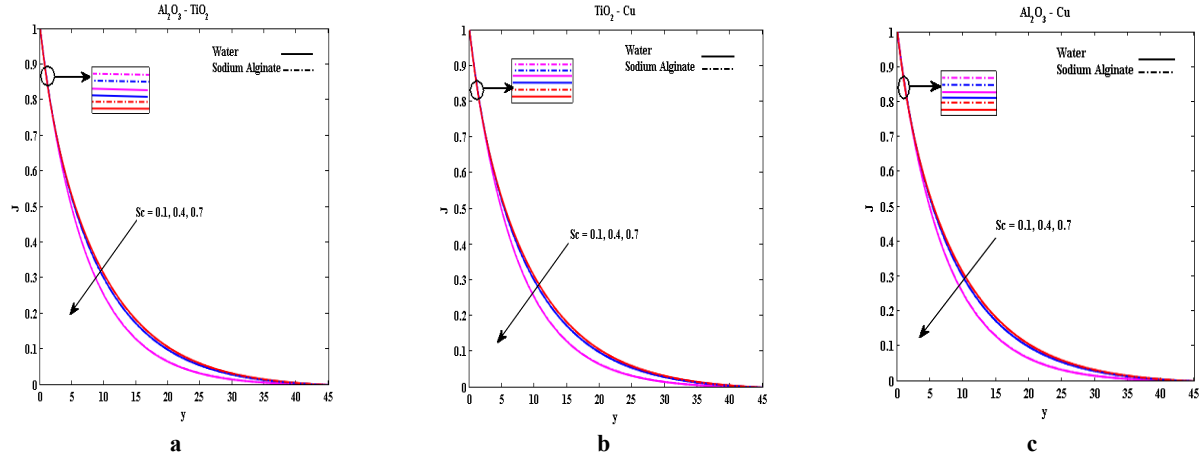

Figure 8. (a-c) Graph of Sc on the microorganism profile

- Graph depict the impact of Schmidt number Sc on the microorganism species density flow fields in hybrid nanofluids. The microorganism species density profiles (Fig. 8(a-c)) decrease with increasing Sc, indicating that advection transport dominates over diffusive transport rates.
- Non-Newtonian base fluids exhibit enhanced kinematic viscosity in concentration and microorganism species density profiles.

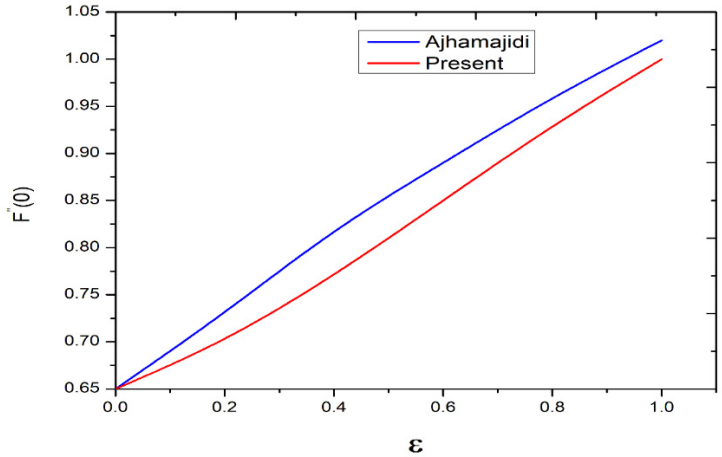

Figure 9. Comparative study of ϵ and $F''(0)$.

Figure 9 and Table 1.

- Demonstrates comparing the current study's results and those published previously [17], showing excellent agreement under limited considerations.
- It Provides numerical values of local Sherwood numbers across three hybrid nanoparticles with two base fluids, categorised by variables such as M, ε, Nc, Nn, and Sc. The local Sherwood number increases with larger values of ε, Nc, Nn, and Sc and decreases with increasing M. Additionally, it is noted that Newtonian base fluids exhibit higher mass transfer rates in Aluminum oxide – Titanium oxide, Titanium oxide – Copper and Aluminum oxide – Copper hybrid nanoparticles.

7. CONCLUSION

This study analysed the magnetic bio-convective flow of Casson hybrid nanofluids through a spinning cone, presenting thermal, mass, and microorganism profiles graphically and tabulating physical quantities. Key findings indicate that an increase in the magnetic parameter (M) enhances heat and motile microorganism profiles, while a more significant spin parameter reduces the temperature profile. The microorganism flow field decreases with increasing Sc values for all hybrid nanofluids. Mass transfer rates in a non-Newtonian base fluid improve with higher β values. For Newtonian base fluids, mass transfer rates increase with ascending ε, Nc, Nn, and Sc. Notably, TiO_2-Cu hybrid nanoparticles exhibit superior Sherwood numbers. The potential applications of hybrid nanofluids in rotating cones span food technology, aeronautical engineering, the pharmaceutical industry, and endoscopy scanning, suggesting future exploration of the benefits and limitations of these nanofluids in such fields.

ORCID

Balaji Padhy, https://orcid.org/0000-0002-3447-2917; **Archana Senapati,** https://orcid.org/0009-0001-7180-5194
Goutam Kumar Mahato, https://orcid.org/0000-0003-4549-0042; **P.K. Rath,** https://orcid.org/0000-0002-3869-9705

REFERENCES

[1] C.K. Ajay, M.A. Kumar, and A.H. Srinivasa, "The effects of thermal radiation, internal heat generation (absorption) on unsteady MHD free convection flow about a truncated cone in presence of pressure work," Materials Today: Proceedings, (2023). https://doi.org/10.1016/j.matpr.2023.05.632

[2] A. Hossain, M.J. Anee, S. Thohura, and M.M. Molla, "Finite difference simulation of free convection of non-Newtonian nanofluids with radiation effects over a truncated wavy cone," Pramana, **97**(4), 168 (2023). https://doi.org/10.1007/s12043-023-02642-w

[3] M.K.A. Mohamed, A.M. Ishak, I. Pop, N.F. Mohammad, and S.K. Soid, "Free convection boundary layer flow from a vertical truncated cone in a hybrid nanofluid," Malaysian Journal of Fundamental and Applied Sciences, **18**(2), 257-270 (2022). https://doi.org/10.11113/mjfas.v18n2.2410

[4] R. Ellahi, A. Zeeshan, A. Waheed, N. Shehzad, and S.M. Sait, "Natural convection nanofluid flow with heat transfer analysis of carbon nanotubes–water nanofluid inside a vertical truncated wavy cone," Mathematical Methods in the Applied Sciences, **46**(10), 11303-11321 (2023). https://doi.org/10.1002/mma.7281

[5] H. Liu, L. Lan, J. Abrigo, H.L. Ip, Y. Soo, D. Zheng, K.S. Wong, *et al*., "Comparison of Newtonian and non-Newtonian fluid models in blood flow simulation in patients with intracranial arterial stenosis," Frontiers in physiology, **12**, 718540 (2021). https://doi.org/10.3389/fphys.2021.718540

[6] G. Aloliga, Y. Ibrahim Seini, and R. Musah, "Heat transfer in a magnetohydrodynamic boundary layer flow of a non-newtonian casson fluid over an exponentially stretching magnetized surface," Journal of Nanofluids, **10**(2), 172-185 (2021). https://doi.org/10.1166/jon.2021.1777

[7] K. Loganathan, M. Sivakumar, M. Mohanraj, and P. Sakthivel, "Thermally radiative Casson fluid flow over a cylinder with Newtonian heating and heat generation/absorption," Journal of Physics: conference series, **1964**(2), 022001 (2021). https://doi.org/10.1088/1742-6596/1964/2/022001

[8] E.O. Fatunmbi, and O.A. Agbolade, "Quadratic Thermal Convection in Magneto-Casson Fluid Flow Induced by Stretchy Material with Tiny Particles and Viscous Dissipation Effects," Physical Science International Journal, **27**(4), 1-11 (2023). https://doi.org/10.9734/psij/2023/v27i4795

[9] U. Shankar, and N.B. Naduvinamani, "Magnetized impacts of Cattaneo-Christov double-diffusion models on the time-dependent squeezing flow of Casson fluid: A generalized perspective of Fourier and Fick's laws," The European Physical Journal Plus, **134**(7), 344 (2019). https://doi.org/10.1140/epjp/i2019-12715-x

[10] A. Raza, M.Y. Almusawa, Q. Ali, A.U. Haq, K. Al-Khaled, and I.E. Sarris, "Solution of water and sodium alginate-based casson type hybrid nanofluid with slip and sinusoidal heat conditions: A prabhakar fractional derivative approach," Symmetry, **14**(12), 2658 (2022). https://doi.org/10.3390/sym14122658

[11] S. Elattar, U. Khan, A. Zaib, A. Ishak, N. Alwadai, and A.M. Abed, "Heat transfer characteristics of cobalt ferrite nanoparticles scattered in sodium alginate-based non-Newtonian nanofluid over a stretching/shrinking horizontal plane surface," Open Physics, **22**(1), 20230182 (2024). https://doi.org/10.1515/phys-2023-0182

[12] M.P. Mkhatshwa, "Overlapping Grid-Based Spectral Collocation Technique for Bioconvective Flow of MHD Williamson Nanofluid over a Radiative Circular Cylindrical Body with Activation Energy," Computation, **12**(4), 75 (2024). https://doi.org/10.3390/computation12040075

[13] Z.A. Alhussain, A. Renuka, and M. Muthtamilselvan, "A magneto-bioconvective and thermal conductivity enhancement in nanofluid flow containing gyrotactic microorganism," Case Studies in Thermal Engineering, **23**, 100809 (2021). https://doi.org/10.1016/j.csite.2020.100809

[14] F.T. Zohra, M.J. Uddin, A.I.M. Ismail, O.A. Bég, and A. Kadir, "Anisotropic slip magneto-bioconvection flow from a rotating cone to a nanofluid with Stefan blowing effects," Chinese journal of physics, **56(**1), 432-448 (2018). https://doi.org/10.1016/j.cjph.2017.08.031

[15] M. Sarfraz, and M. Khan, "Cattaneo-Christov double diffusion-based heat transport analysis for nanofluid flows induced by a moving plate," Numerical Heat Transfer, Part A: Applications, **85**(3), 351-363 (2024). https://doi.org/10.1080/10407782.2023.2186551

[16] A. Hussanan, M. Qasim, and Z.M. Chen, "Heat transfer enhancement in sodium alginate based magnetic and non-magnetic nanoparticles mixture hybrid nanofluid," Physica A: Statistical Mechanics and its Applications, **550**, 123957 (2020). https://doi.org/10.1016/j.physa.2019.123957

[17] M. Aghamajidi, M. Yazdi, S. Dinarvand, and I. Pop, "Tiwari-Das nanofluid model for magnetohydrodynamics (MHD) natural-convective flow of a nanofluid adjacent to a spinning down-pointing vertical cone," Propulsion and Power Research, **7**(1), 78-90 (2018). https://doi.org/10.1016/j.jppr.2018.02.002

[18] Z.A. Alhussain, A. Renuka, and M. Muthtamilselvan, "A magneto-bioconvective and thermal conductivity enhancement in nanofluid flow containing gyrotactic microorganism," Case Studies in Thermal Engineering, **23**, 100809 (2021). https://doi.org/10.1016/j.csite.2020.100809

МАГНІТОГІДРОДИНАМІЧНИЙ ТА БІОКОНВЕКЦІЙНИЙ ВПЛИВ НА ГІБРИДНУ ДИНАМІКУ НАНОРІДИН НАД ПЕРЕВЕРНУТИМ ОБЕРТОВИМ КОНУСОМ З РІЗНИМИ ОСНОВНИМИ РІДИНАМИ

Баладжі Падхі[a], Арчана Сенапаті[b], Гутам Кумар Махато[a], П.К. Рат[a]

[a]*Університет технології та управління Центуріон, Одіша, Індія*

[b]*Факультет математики школи прикладних наук KIIT Deemed to be University, Бхубанешвар, Одіша, Індія.*

У цій роботі досліджується комбінований вплив магнітогідродинаміки (МГД) і біоконвекції на динаміку потоку гібридних нанофлюїдів над перевернутим обертовим конусом з різними базовими рідинами. Гібридні нанофлюїди, що складаються з наночастинок, суспендованих у різних базових рідинах, демонструють унікальні теплові та текучі характеристики завдяки взаємодії між магнітними полями та явищами біоконвекції. Основні рівняння, що включають принципи МГД та біоконвекції, отримані та розв'язані чисельними методами. Аналіз розглядає вплив ключових параметрів, таких як напруженість магнітного поля, швидкість обертання конуса, об'ємна частка наночастинок і типи базових рідин на поведінку потоку, теплопередачу та стабільність системи. Результати показують, що МГД суттєво впливає на профілі швидкості та температури гібридних нанофлюїдів, тоді як біоконвекція сприяє підвищенню швидкості змішування та теплопередачі. Крім того, вибір базової рідини відіграє вирішальну роль у визначенні загальної продуктивності гібридної системи Nano fluid. Це дослідження дає цінну інформацію щодо оптимізації дизайну та роботи систем, що використовують гібридні нанофлюїди в програмах, де МГД та біоконвекційні ефекти є помітними.

Ключові слова: *магнітогідродинаміка (МГД); біоконвекція; гібридні нанофлюїди; перевернутий обертовий конус; базові рідини; наночастинки; динаміка течії*